Engineering and Technology Journal
Journal homepage: engtechjournal.org

Nonlinear Finite Element Analysis of Fiber Reinforced Concrete Slabs

Saad A. Al-Taan [a*], **Ayad A. Abdul-Razzak** [b]

[a] Mosul University, Al-Majmo'a Al-Thqafia, Mosul, Iraq. saad.altaan@yahoo.com

[b] Mosul University, Al-Majmo'a Al-Thqafia, Mosul, Iraq. drayad_aghwan@yahoo.co.uk

*Corresponding author.

Submitted: 16/03/2020 Accepted: 20/04/2020 Published: 25/03/2021

K E Y W O R D S

Finite element, nonlinear analysis, reinforced concrete slabs, shear modulus, steel fibers, tension stiffening

A B S T R A C T

This paper presents a study on the behavior of fiber reinforced concrete slabs using finite element analysis. A previously published finite element program is used for the nonlinear analysis by including the steel fiber concrete properties. Concrete is represented by degenerated quadratic thick shell element, which is the general shear deformable eight node serendipity element, and the thickness is divided into layers. An elastic perfectly plastic and strain hardening plasticity approach are used to model the compression behavior of concrete. The reinforcing bars were smeared within the concrete layers and assumed as either an elastic perfectly plastic material or as an elastic-plastic material with linear strain hardening. Cracks initiation is predicted using a tensile strength criterion. The tension stiffening effect of the steel fibers is simulated using a descending parabolic stress degradation function, which is based on the fracture energy concept. The effect of cracking in reducing the shear modulus and the compressive strength of concrete parallel to the crack direction is considered. The numerical results showed good agreement with published experimental results for two fibrous reinforced concrete slabs.

How to cite this article: S. A. Al-Taan, and A. A. Abdul-Razzak, "Nonlinear Finite Element Analysis of Fiber Reinforced Concrete Slabs," Engineering and Technology Journal, Vol. 39, Part A, No. 03, pp. 426-439, 2021.
DOI: https://doi.org/10.30684/etj.v39i3A.1641
This is an open access article under the CC BY 4.0 license http://creativecommons.org/licenses/by/4.0

1. INTRODUCTION

Reinforced concrete slabs are important structural members in any reinforced concrete building, since it is the only member that takes the live loads directly. The thickness of the flat plate or flat slab is mostly controlled by the punching shear stresses created at the slab-column connection. To prevent the catastrophic and brittle punching shear failure, the ACI Code (318-19) [1] recommend the increase of

Publishing rights belongs to University of Technology's Press, Baghdad, Iraq.

the slab thickness or use of shear reinforcement. The shear reinforcement may be in the form of single leg, multiple legs, bent-down bars, shear studs, or shear head reinforcement.

Steel, glass, polymer, and other types of short discrete fibers have been added as reinforcement to concrete, thus producing a composite material with enhanced tensile strength, ductility, well defined post cracking behavior, and strain capacity [2,3]. The ACI Code (318-19) [1] recommends the use of deformed steel fibers complying with ASTM Specifications [4] as shear reinforcement with length to diameter ratio ranging between 50 and 100. Steel fibers have been used to improve the flexural and shear resistance of reinforced concrete slabs [5-11].

Nonlinear finite element (FE) analysis is used extensively for the analysis of fiber reinforced concrete (FRC) members [12-14]. Geometrical and material nonlinearity due to tensile cracking, bond-slip between the tension reinforcement bars and the surrounding concrete, nonlinear behavior of concrete in compression have been considered. The nonlinear (FE) is used also by many researchers for analysis of fiber reinforced concrete slabs [11,15-21].

Six (FRC) slabs were cast, and tested by Alvarez [19], the slabs were 3.0 (m) of length and 200 (mm) thickness and three different widths, 1.5, 2.0, and 3.0 (m). Hooked steel fibers 50×0.62 (mm) was used with a volume fraction of 0.5%. The slabs were then analyzed using the software ATENA for the nonlinear analysis. The expression suggested by Barros and Figueiras [22] is used for the SFRC in uniaxial compression. Concrete in tension modelled using nonlinear fracture mechanics combined with the crack band method and the smeared crack approach using a tri-linear diagram. Tetrahedral solid elements were used for meshing the slabs. Cracks patterns were predicted with acceptable accuracy, and an overestimation of the experimental results was observed for all the slabs.

Eight high strength steel fiber reinforced concrete slabs that were tested by Yaseen [7] analyzed by Sayhood et al. [20] using the program (P3DNFEA) for the nonlinear (FE). Concrete is represented by 20-node quadratic brick elements, and the reinforcing bars was simulated by embedded axial elements. In compression, concrete is assumed to follow an elastic-plastic work hardening model followed by a perfectively plastic response, which ended at the onset of crushing. A parabolic equivalent uniaxial stress-strain curve has been used to simulate the work hardening stage of behavior and the plastic strain is controlled by an associated flow rule. Concrete in tension assumed to behave elastically up to the cracking strain, followed by three descending trilinear lines for (FRC). A shear retention model is used to simulate the effect of cracking on the shear strength normal to the crack's direction. The average ratio of the numerical to the experimental failure loads was 0.915 with a standard deviation of 0.027.

Abdel-Rahman et al. [11] tested fourteen reinforced concrete slabs reinforced longitudinally with 1.2% in both directions under concentric and eccentric load. Steel fibers with dimensions (50×0.52×0.72 mm) and volume fractions of 0.5 to 1.5% were used to study the influence of steel fibers on the punching shear strength of the slabs. The test results showed an increase in the punching shear strength up 24%. A nonlinear (FE) analysis is conducted using the program ANSYS R14.5 to compare the numerical with the experimental results. Concrete is represented by eight node solid elements, solid65, and three-dimensional link elements 180 were used to simulate the reinforcing bars. The average ratio of the numerical to the experimental load is 0.98 with a standard deviation of 0.14, which indicates an excellent agreement.

Puddicome[21] presented a (FE) model using the program ABAQUS for the analysis of (FRC) slabs. Concrete damaged Plasticity constitutive model is used to model the nonlinear behavior of concrete. The tension – stiffening effect is modelled using an exponential decay expression with variables to account for varying concrete grades, flexural reinforcement ratio, concrete of steel fibers in the concrete mix, and the yield strength of steel. Eight-nodded hexahedral (brick) elements were used to model concrete with reduced integration, and the reinforcement is modeled as two-node linear truss elements. The model is calibrated using the test results from nine slabs from the literature, and the ratio of the numerical to the experimental failure load varied from 0.78 to 1.281 with an average ratio of 1.068 and a standard deviation of 0.195.

In this paper,the computer program of Ref. [23] for the nonlinear analysis of reinforced concrete plates and shells is modified in this study by including the constitutive material relationships of steel fiber concrete is used for the nonlinear (FE) analysis of (FRC) slabs under increasing monotonic loading. Modified version of the Newton-Raphson method has been used for the solution of the nonlinear problem.

1. MATERIALS CONSTITUTIVE RELATIONSHIPS

I. Compression

The first part of the curve in compression can be treated using the elasticity theory, Figure 1, and the second part using the theory of plasticity. The growth of the yield surface during plastic loading is used to model the hardening phenomena. The mean normal stress, I1 and the shear stress invariant, J2 is used as dependent variables for the yield function:

$$f(I_1,J_2) = \sqrt{\beta_f(3J_2) + \alpha_f I_1} = \sigma_o \quad (1)$$

where α_f and β_f are material parameters, and σo is the equivalent effective stress, taken as the compressive strength f'cf of fibrous concrete. For the biaxial compression state:

$$\sigma_1 = \sigma_2 = \omega f'_{cf} \quad (2)$$

ω is the biaxial stress ratio ($\omega = \sigma_1/\sigma_2$)

The experimental results reported in Refs. [24-26] is used in a regression analysis, and the following relationship is used taking into account the influence of the ratio of stresses, aspect ratio and volume fraction of steel fibers, then equals to [27]:

$$\omega = e^x \quad (3)$$

$$x = 1/[(3.339 - 0.9772\ln(V_f L_f/D_f)] \quad (4)$$

α_f and β_f can be expressed as follow:

$$\alpha_f = \frac{\sigma_o(1-\omega^2)}{\omega^2-2\omega} \quad (5)$$

$$\beta_f = (1-2\omega)/(\omega^2-2\omega) \quad (6)$$

the stress components can then be used in the yield function and can be written as:

$$f(\sigma) = \left[\beta_f\{(\sigma_x^2 + \sigma_y^2 + \sigma_{xy}) + 3(\tau_{xy}^2 + \tau_{xz}^2 + \tau_{zy}^2)\} + \alpha_f(\sigma_x + \sigma_y)\right]^{1/2} (7)$$

To predict the crushing state of concrete, the yield criterion is converted into strain instead of stress components. The experimental results reported by [24-26] are used to estimate the ultimate compression strain of steel (FRC), [27]:

$$\epsilon_{cfu} = 0.003011 + 0.002295V_f \quad (8)$$

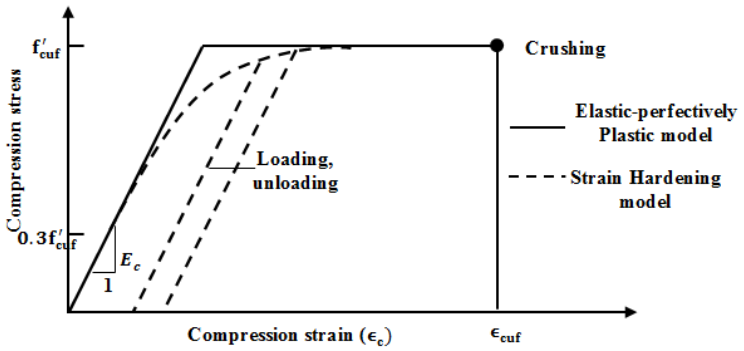

Figure 1: Stress-strain relationships for fibrous concrete in uniaxial compression [27]

II. Tension

As for plain concrete, the initial part of the stress-strain curve in tension, up to first cracking, Figure 2 is linear. Then it deviates from linearity due to micro-cracks initiation and propagation. This is followed by a formation of an unstable micro-crack system, which grows rapidly under the tensile stress bringing the material to its post-peak region [28]. The equations derived by Soroushian and Lee [29] for the tensile strength f'tf and its corresponding strain □tf for (FRC) are used in this study:

$$f'_{tf} = f'_t(1 + 0.016N_f^{\frac{1}{3}} + 0.05\pi D_f L_f N_f) \quad (9)$$

$$\epsilon_{tf} = \epsilon_t\ (1 + 0.35 D_f L_f N_f) \quad (10)$$

where Nf is the number of fibers crossing a unit area [30]:

$$N_f = 1.64 V_f/(\pi D_f^2) \quad (11)$$

After the formation of a continuous crack, a stress drop occurs, and the crack is arrested at a certain level by the pullout resistance of the fires. It is assumed that the fibers bridging the crack start resisting the applied stress immediately after composite cracking.This stress is defined as fu. The post cracking tensile strength fu can thus be calculated as the product of the average bond stress and the interfacial area of fibers bridging the cracked section [28]:

$$f_u = \eta_o \tau_u V_f L_f / D_f \quad (12)$$

where η_o is the orientation factor representing the percentage of fibers aligned in a certain direction. Different values were proposed for this factor like (1/3, 0.41, and 0.5), the probabilistic value of 0.41 is used in this study [30]. τu is the average bond strength and is equal to [29]:

$$\tau_u = 2.62 - 0.0036 N_f \quad (13)$$

After the sudden drop in stress from ftf' to fu a descending nonlinear stress-strain relationship is adopted in the present study to simulate the post-peak constitutive model as shown in Figure 2. The derivation of the nonlinear curve is based on the fracture energy concept [27] using experimental load-deformation curve reported by Visalvanich and Naaman [31]. The stress-strain relation can be expressed as follows:

$$\sigma_i = f_u\left[(\epsilon_i - \epsilon_m)/(\epsilon_{tf} - \epsilon_m)\right]^2 \quad (14)$$

where ε_m is the limiting tensile strain. This value is calculated [27] assuming that the descending stress-strain curve is similar to that of a load- displacement curve of a fiber exhibiting pull-out, and the area under this curve is equal to the fracture energy Gf:

$$\epsilon_m = 3G_f/(hf_u) + \epsilon_{tf} \quad (15)$$

h is the Gauss pointcharacteristic length. The fracture energy Gf which is derived by Visalvanich and Naaman [31] is adopted in this study:

$$G_f = 0.171\beta\tau_u V_f\left(2L_f^2/D_f\right) \quad (16)$$

The tension stiffening effect is considered as indicated in Figure 2 by assuming a gradual release of the concrete stress component normal to the cracked plane. Unloading and reloading of cracked concrete is supposed to follow the linear behavior shown in Figure 2 with a fictitious secant modulus Ets.

In the biaxial tension-compression zone, the parabolic relationship derived by Al-Taan and Mahmood [32] is used:

$$\sigma_{2p} = \left[\left(\sqrt{1 + 4(\alpha_2^2 S^2)} - 1\right)/(2\alpha_2^2 S^2)\right] f'_{cf} \qquad (17)$$

S = f'cf / ftf, and the peak tensile strength as:

$$\sigma_{1p} = \sigma_{2p}\alpha_2 2 \qquad (18)$$

where σ1p and σ2p are the limiting principal tensile and compressive strengths respectively in this zone and α2 is the principal stress ratio = σ_2/σ_1.

When cracking occurs, the concrete is assumed to be in a state of uniaxial compression parallel to the cracks and exhibiting characteristics of the strain hardening elasto-plastic model. After cracking the relationship proposed by Vecchio and Collins [33] is adopted:

$$f'_{cfmax} = f'_{cf}/(0.8 + \frac{0.34\epsilon_1}{\epsilon_2}) \leq f'_{cf} \qquad (19)$$

In the direction perpendicular to the crack,the elastic modulus and Poisson's ratio is reduced to zero and a reduced shear modulus is employed to simulate the aggregate interlock.

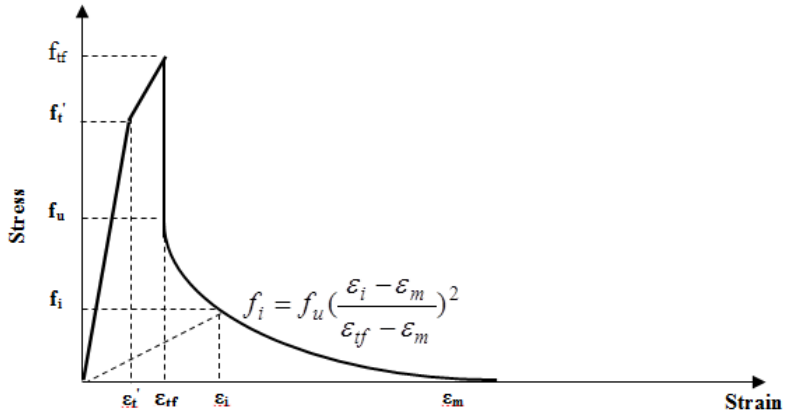

Figure 2: Stress-strain curve for fibrous concrete in tension [27]

III. Shear Modulus of Cracked Concrete

Four different expressions are used to reduce the shear modulus, Figure 3: Shear Modulus of Cracked Concrete

Four different expressions are used to reduce the shear modulus, Figure 3:

Approach G1, in this approach the value of is linearly decreasing with the current tensile strain as assumed by Cedolin and Poli [34], Figure 3, if cracks appeared in direction 1,

$$\bar{G}_{12} = 0.25G(1 - \epsilon_1/\epsilon_m) \qquad \text{for} \quad \epsilon_1 < \epsilon_m \quad (20a)$$

$$\bar{G}_{12} = 0 \qquad \text{for} \quad \epsilon_1 \geq \epsilon_m \quad (20b)$$

Biaxial orthotropic approach G2: This approach has been proposed by Chen [35]. The shear modulus of cracked concrete can be written as follows:

$$\bar{G}_{12} = E_1 E_2/(E_1 + E_2 + 2\upsilon E_2) \qquad (21)$$

If Poisson's ratio (υ) equal to zero Eq. (21) becomes:

$$\bar{G}_{12} = E_1 E_2/(E_1 + E_2) \qquad (22)$$

where E1 and E2 are the elastic moduli in directions 1and 2 respectively.

Approach G3: In this approach the value of G is parabolically decreasing with the current tensile strain, using a function similar to that used in Eq. (14), [27], if the cracks appeared in direction 1,

$$\bar{G}_{12} = 0.25G[(\epsilon_1 - \epsilon_m)/(\epsilon_{tf} - \epsilon_m)]^2 \qquad \text{for} \quad \epsilon_1 < \epsilon_m \quad (23a)$$

$$\bar{G}_{12} = 0 \text{for} \epsilon_1 \geq \epsilon_m \quad (23b)$$

Approach G4: This approach was proposed initially proposed by [36] and modified in this study by substituting $\varepsilon_{tf}$for ε_t. The shear modulus of concrete cracked in direction 1, can be calculated as follows:

$$\bar{G}_{12} = 0.4G/(\epsilon_1/\epsilon_{tf}) \qquad (24)$$

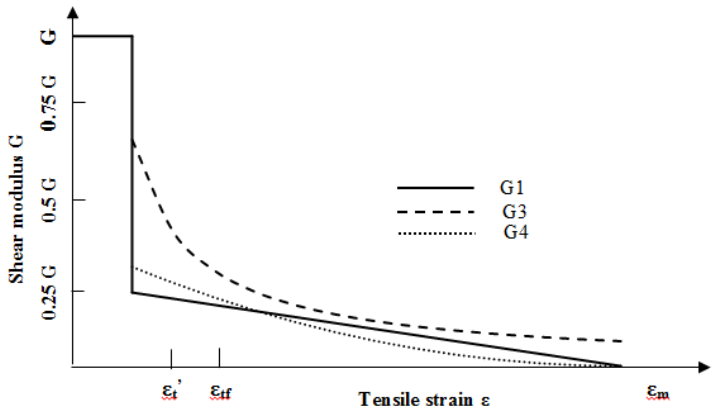

Figure 3: Reduced shear moduli

2. FINITE ELEMENT FORMULATION

The eight-node serendipity thick shell element is used in the present study to represent the slabs. Three displacements and two independent rotations of the normal to the element mid surface are considered for each node. The formulations of this element are mentioned by Onate et al. [37]. This element is the most popular degenerated shell element in isoparametric formulation, and it is the simplest element considered in the original work of Ahmad [37], and this element requires C0 continuity. Shear locking occurs even in moderately thin situations when using full integration. A great improvement of the results was obtained when the reduced integration was used [37]. The element can be divided into a number of concrete layers through the thickness. The stresses of each layer are computed at the Gauss points and assumed to be constant. Smeared approach is implemented for the steel reinforcement which is incorporated with the layered approach.

3. NUMERICAL EXAMPLES

Two examples were analyzed, the first one (FS-20) is a square lightweight (FRC) slab tested by Theodorakopoulos and Swamy [6], and the second one (S-2) is a square normal (FRC) slab-column connection tested by Swamy and Ali [5]. Both slabs were with a side length of 1.8 m and 125 mm thick provided with a central square column stub. One quarter of each slab is analyzed due to symmetry, Figure 4. Dimensions, reinforcement details and loading are shown in Figure 4a. The material properties for the first slab are summarized in Table I.

A convergence study is conducted on the optimum number of elements and layers. The slabs were modelled in the present study by three meshes containing four, nine, and eleven elements. However, the loading, geometry of the slab, and the obtained results showed that using eleven elements as shown in Figure 5 gave a reliable simulation and results. The number of layers were varied from 3 to 10, to find the optimum number to be used in the analysis. The numerical results

show that the optimum number of layers that give the best agreement with the experimental results is 10 as will be shown later.

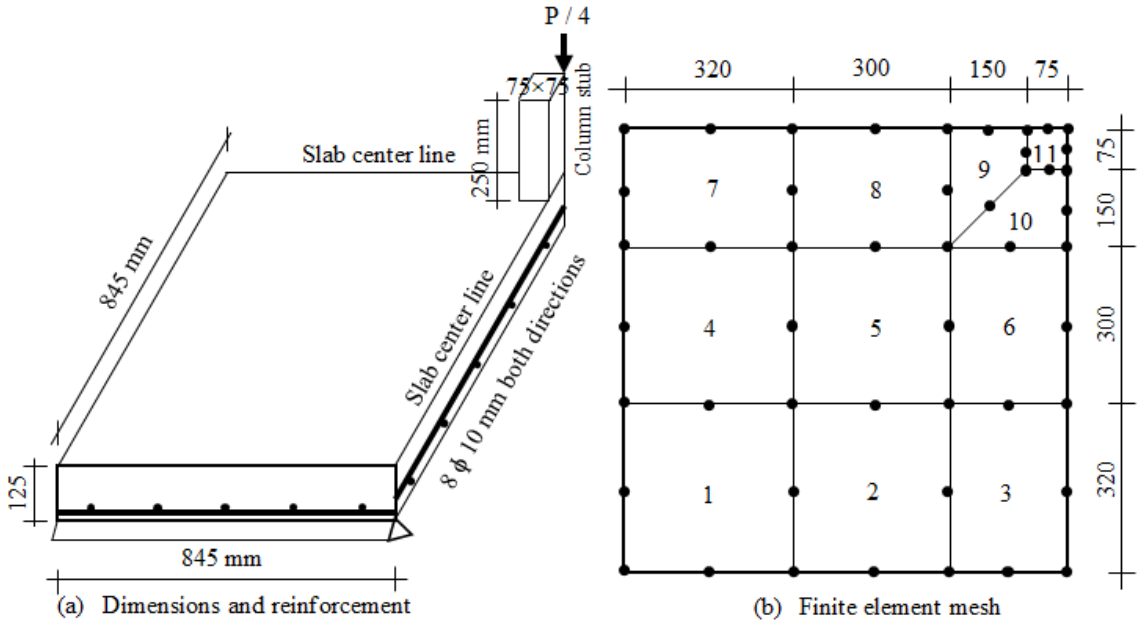

Figure 4: Details and finite element mesh for slab FS-20, (a) Dimensions and reinforcement, (b) Finite element mesh

Table I: Materials properties of slab FS-20 [6]

E_{cf}(GPa)	$E_s^{'}$ (GPa)	V_f^{*} %	$f_{cuf}^{'}$ (MPa)	$f_t^{'}$ (MPa)	f_y (MPa)	A_s bars	$\epsilon_{cuf}^{**} \times 10^{-3}$
19.4	17	1.0	46.3	4.38	425	8-ϕ 10	5.3

* Crimped steel fibers 0.5×50 (mm), ** calculated from Eq. (8), $\nu_c = 0.15$, $E_s = 204$ GPa.

Figure 5 shows the load-deflection for slab (FS-20) with 3, 4, 5, 6, 8, and 10 layers across the depth using models G3 and G4 for reducing the shear moduli. The Figures showed that the 10 layers simulation gave the best agreement with the experimental results for both G models. The four reduced shear modulus relationships, Eqs. (20-24) were used in the analysis of the same slab to check their suitability for the analysis of (FRC) slabs. Figures 6a and 6b show the load-deflection curves using the elasto-plastic and strain hardening respectively to model concrete together with all the G models. The Figures showed that in the pre-yield stage all the proposed G models gave good agreement with the experimental results and in general there is no remarkable difference in the behavior at this stage for all the proposed G models. In the post-yield stage, the models G1 and G3 gave good agreement with the experimental results but overestimated the failure load. Model G2 underestimated the ultimate loads, and G4 gives good agreement with the experimental results specially with the value of ultimate load (numerical ultimate load = 210.94 kN versus the experimental ultimate load = 211 kN).

Figure 6 also show that using elastic-plastic and strain hardening models, does not yield considerable difference in the results, and this may be attributed to the relatively small compression stresses developed in the compression zone prior to final failure since the slab is under reinforced (reinforcement ratio = 0.37%).

Figure 7 shows that the full integration rule for both models G3 and G4 give slightly a larger ultimate load than the ultimate load obtained using these models with reduced integration. The locking phenomena does not occur because (span/thickness) equals to 13.5 [23].

Initial damage to the slab occurred in the form of tension cracking in the radial direction Figures 8 and 9. With increasing load, cracks propagate extensively through the depth and in the radial direction and in the circumferential direction in region close to the column stub, Figure 8. Such distribution of cracks forms a mechanism of flexural failure similar to what is assumed in yield line analysis (circular fans). Figures 8 and 10 show the region where crushing occurred near the loaded area, cracked zone in one or two direction and the uncracked zone. The Figures show that the plastic zone spread over about 3 % of the total area of the slab.

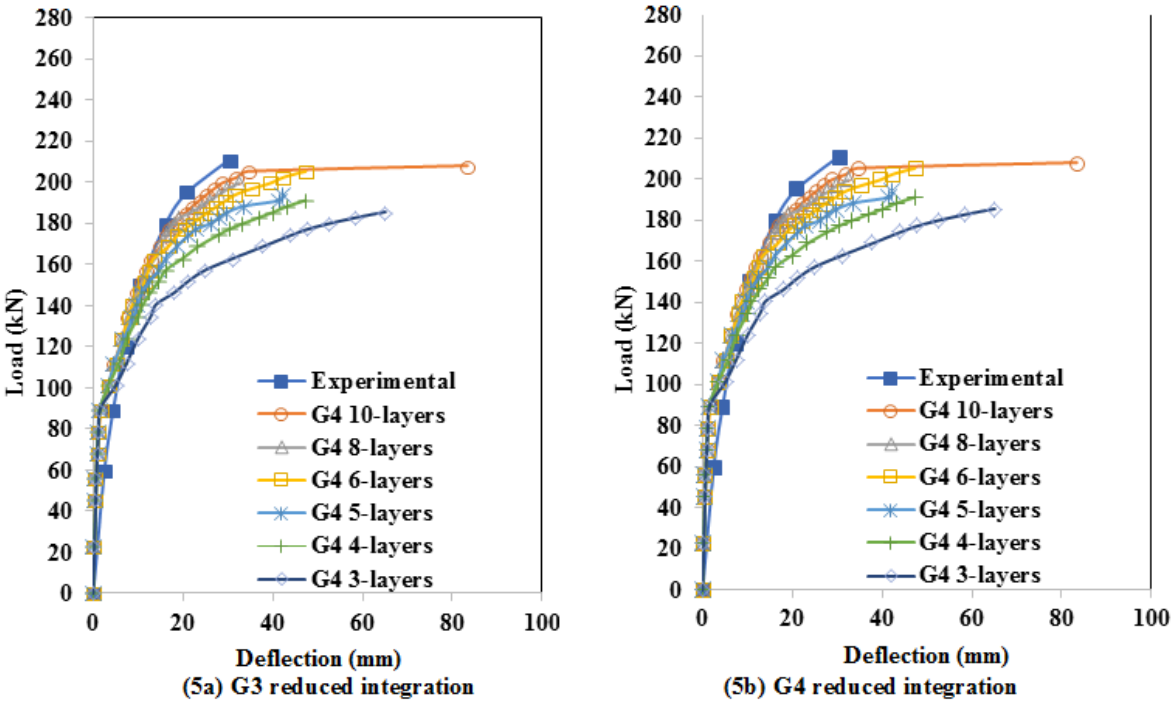

Figure 5: Experimental and numerical load-deflection curves for slab FS-20 using different number of layers, (a) G3 model, (b) G4 model

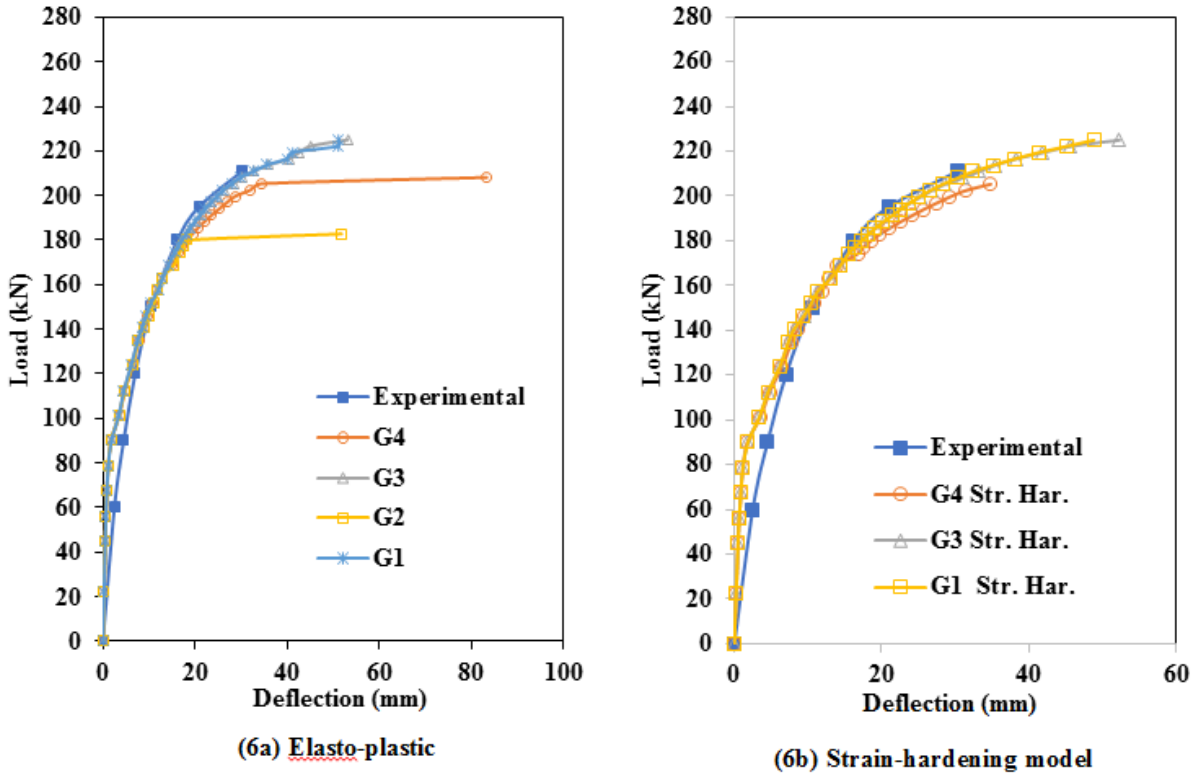

Figure 6: Experimental and numerical load-deflection curves for slab FS-20 using elasto-plastic and strain hardening models, (a) Elasto-plastic model, (b) Strain hardening model

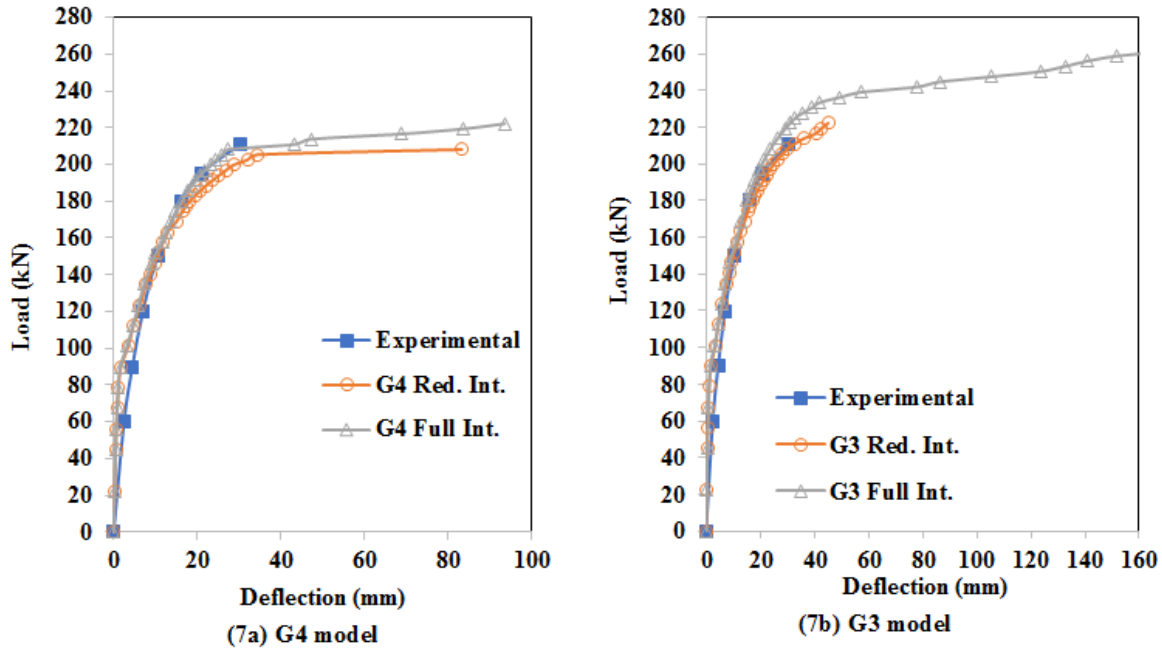

Figure 7: Experimental and numerical load-deflection curves for slab FS-20 using full and reduced integration, (a) Full integration, (b) Reduced integration

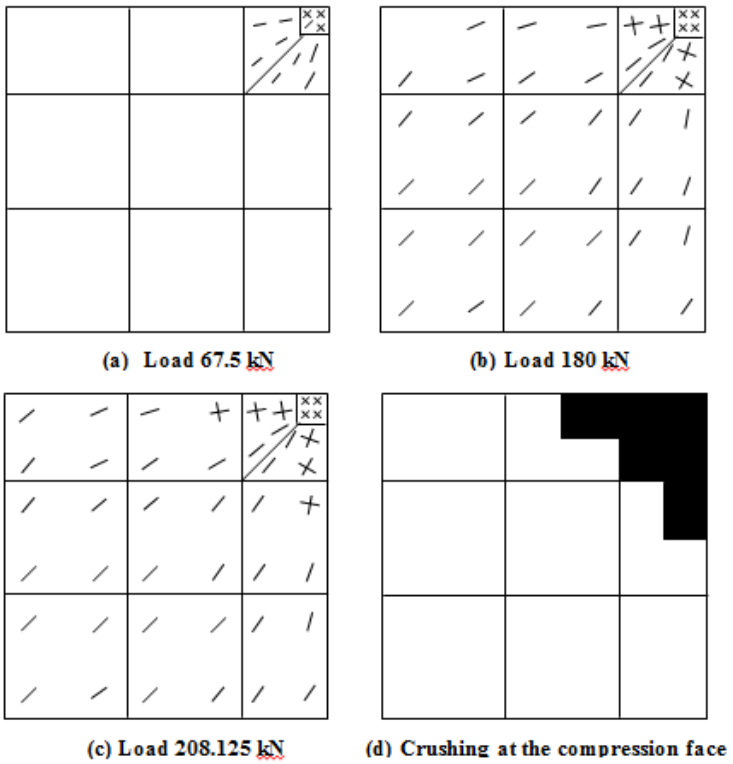

Figure 8: Cracking patterns and crushing, (a) Cracking at load 67.5 kN, (b) Cracking atload 180 kN, (c) Cracking at load 208.125 kN, (d) Crushing at the compression face

Figure 9: Experimental crack pattern of slab FS-20 [6]

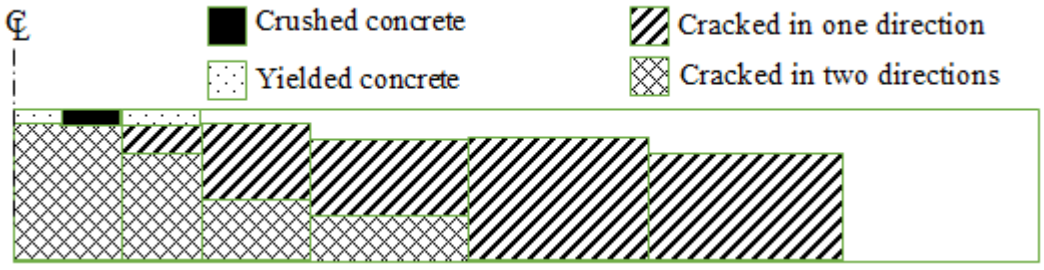

Figure 10: Profile of cracked and damaged zone at load 205.3 kN

The second example S-2 is a square normal (FRC) slab-column connection tested by Swamy and Ali [5] with the same dimensions as Example (1) FS-20, Figure 4. The slab was designed to fail in shear and incorporated 0.5×50 mm crimped steel fibers at volume of 0.5%. The material properties of the tested slab are summarized in Table II. The reinforcement in tension and compression were represented by two steel layers respectively and six concrete layers are found to be enough for the analysis.

Table II: Materials properties of slab S2 [5]

E_{cf}(GPa)	E_s' (GPa)	V_f^* %	f_{cuf}' (MPa)	f_t' (MPa)	f_y (MPa)	A_s' bars	A_s bars	ϵ_{cuf}^{**} $\times 10^{-3}$
33.29	17	0.5	34.87	4.2	425	7- ϕ 8	12-ϕ 10	4.4

* Crimped steel fibers 0.5×50 mm, ** calculated from Equation (8), νc = 0.15.

Figure 11 shows the load-deflection curves, all the G models gave good agreement with the experimental results prior to failure, but G2 and G4 models give lower values of failure load while G1 and G3 models give higher value of failure load.

Figure 12a shows the load tensile steel strain curve near midspan for the experimental and the numerical values using G4 with strain hardening model and reduced integration rule. It is clear from this figure that the numerical results have a good agreement with the experimental values especially in the post cracking stage up to the ultimate load. Figure 12b shows the load compression steel strain curves near midspan using also G4 with strain hardening model and reduced integration rule. It is clear from this figure that below a load of about 100 kN, the strain is compression. Then, the neutral surface is rising and the steel becomes in the tension zone. A reasonable agreement can be noticed between experimental and numerical values of strain.

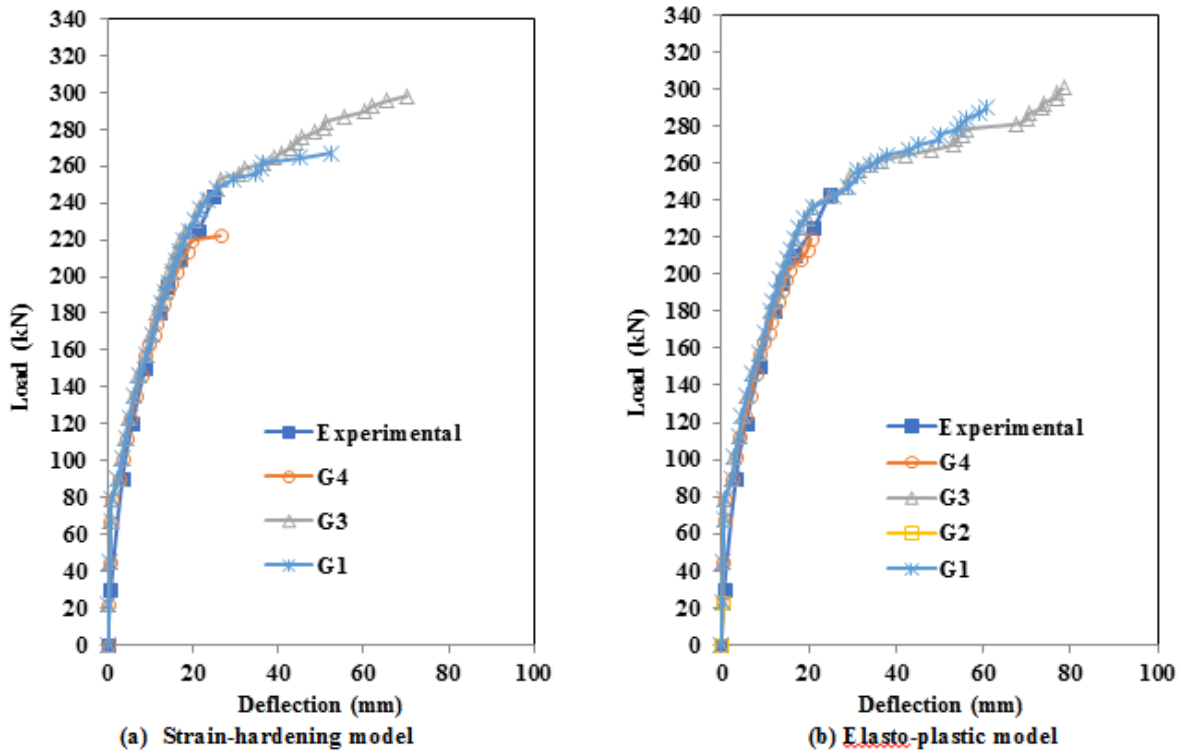

Figure 11: Load-deflection curves for slab S-2, (a) Strain hardening model, (b) Elasto-plastic model

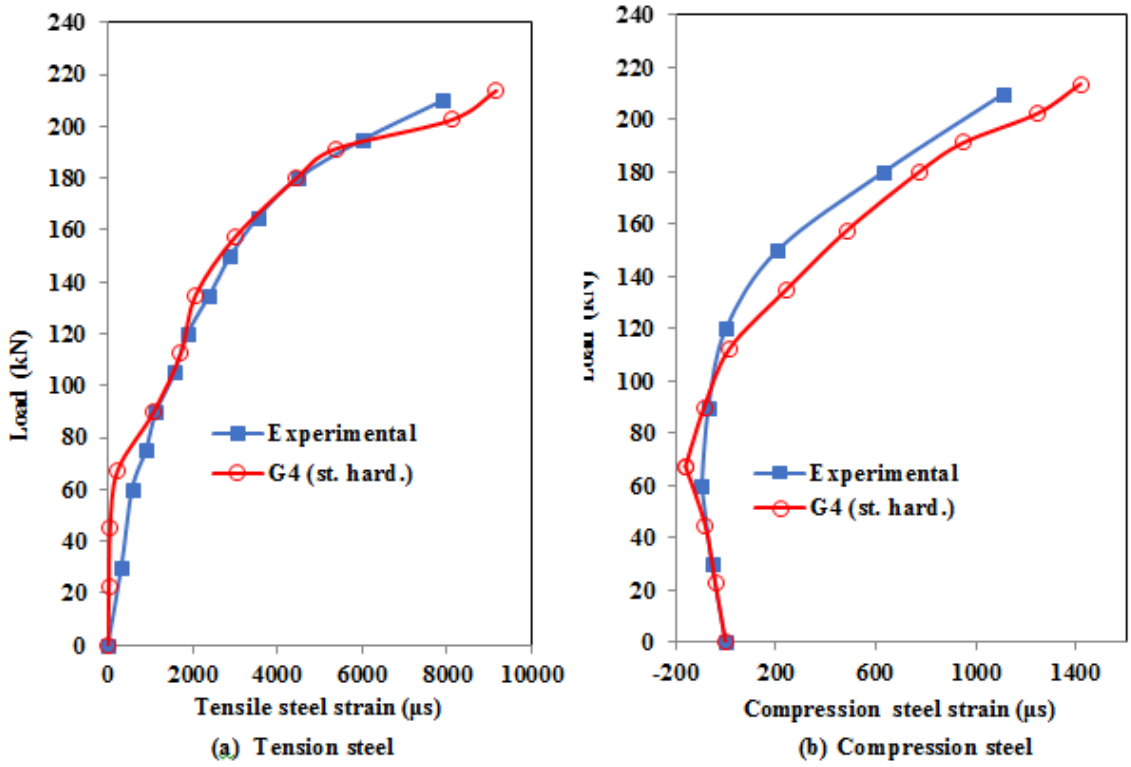

Figure 12: Load-steel strains curves for slab S-2, (a) Tension steel, (b) Compression steel

4. CONCLUSIONS

The adopted constitutive materials relationships with the finite element results showed a good agreement with the experimental results which includes cracks initiation and propagation, deflection,

Steel strains, and load capacities for both lightweight and normal weight (FRC) slabs. The eight nodded (Serendipity) general shear deformable shell elements with five degrees of freedom showed good performance for the nonlinear analysis of normal weight and lightweight (FRC) slabs. Shear reduced modulus G2 and G4 showed better agreement for the failure load than G1 and G3. The proposed method can be used as a design guide for other cases. Refined materials constitutive relationships may give numerical results that may agree better with the experimental results.

References

[1] ACI Committee 318-19, "Building Code Requirements for Structural Concrete and Commentary," American Concrete Institute, Farmington Hills, MI, 48331, USA, 2019.

[2] ACI Committee 544, "Report on Fiber Reinforced Concrete, Reported by ACI Committee 544," American Concrete Institute, Farmington Hills, MI, 48331, USA, 2002.

[3] ACI Committee 544.4R, "Guide to Design with Fiber-Reinforced Concrete," ACI Committee 544," American Concrete Institute, Farmington Hills, MI, 48331, USA, 2018.

[4] ASTM A820M-16, Standard Specification for Steel Fibers for Fiber-Reinforced Concrete, ASTM International, West Conshohocken, 2016.

[5] R. N. Swamy, and S. A. R. Ali, "Punching Shear Behavior of Reinforced Concrete Slab – Column Connections Made with Steel Fibers Concrete," ACI Jour., Vol. 79, No. 5, pp. 392 – 406, May 1982.

[6] D. D. Theodorakopoulus, and R. N. Swamy, "Contribution of Steel Fibers to the Strength Characteristics of Lightweight Concrete Slab – Column Connections Failing in Punching Shear, " ACI Structural Jour., Vol. 90, No. 4, pp. 342 – 355, April 1993.

[7] A. A. Yaseen, Punching Shear Strength of Steel Fiber High Strength Reinforced Concrete Slabs," M.Sc. Thesis, Department of Civil Engineering, University of Salahaddin, 2006, 111pp.

[8] L. N. Minh, M. Rovnak, T. T. Quoc, and K. N. Kim, "Punching Shear Resistance of Steel Fiber Reinforced Concrete Slabs," Procedia engineering, pp. 1-8, Dec. 2011.

[9] V. B. Jatale, and L. G. Kalurkar, "Punching Shear High Strength Steel Fiber Reinforced Concrete Slabs," Inter. Jour. of Engineering Research and Applications, pp. 269-275, Vol.3, No. 6, Nov.-Dec. 2013.

[10] T. K. Tan, and A. Venkateshwaran," Punching Shear in Steel Fibre Reinforced Concrete Slabs without Traditional Reinforcement," IOP Conference Series: Materials Science and Engineering, 246, pp.1-9, 2017.

[11] A. M. Abdel-Rahman, N. Z. Hassan, and A. M. Soliman," Punching Shear Behavior of Reinforced Concrete Slabs using Steel Fibers in the Mix," Housing and Building National Research Center Jour. (Egypt), Vol. 14, pp. 272-281, 2018.

[12] S. A. Al-Taan, and N. A. Ezzadeen," Nonlinear Finite Element Analysis of Steel Fibre Reinforced Concrete Members," Proc. Of the Inter. Conf. on Fibre Reinforced Cement and Concrete, pp. 435-446, July,1992.

[13] S. A. Al-Taan, and N. A. Ezzadeen," Flexural Analysis of Reinforced Fibrous Concrete Members Using the Finite Element Method," Jour. of Computers and Structures, Vol. 56, No. 6, pp. 1065-1072, Sept. 1995.

[14] A. A. Abdul-Razzak, and S. A. Al-Ta'an," Nonlinear Finite Element Analysis of Fibrous Reinforced Concrete Deep Beams," Al-Rafidain Engineering Jour., (Iraq), Vol. 11, No. 1, pp. 47-62, January 2003.

[15] A. A. Abdul-Razzak, and N. E. Aljbure," A Nonlinear Analysis of Fibrous Reinforced Concrete Slabs by Assumed Strain and Heterosis Elements," Al-Rafidain Engineering Jour., (Iraq), Vol. 18, No. 5, pp. 14-23, 2010.

[16] Z. Tazaly," Punching Shear Capacity of Fibre Reinforced Concrete Slabs with Conventional Reinforcement: Computational Analysis of Punching Models," M.Sc. Thesis, Royal Institute of Technology (KTH), Dept. of Civil and Architectural Engineering, 2012, Stockholm, Sweden.

[17] S. O. Mpegetis," Behavior and Design of Steel Fibre Reinforced Concrete Slabs," Ph.D. Thesis, Imperial College of Science and Technology, 2012, Britain.

[18] F. Irani, and B. M. Abadi," Finite Element Analysis of Conventional and Fiber Reinforced Concrete Slabs," M.Sc. Thesis, Chalmers University of Technology, 2013, Sweden.

[19] A. B. Álvarez," Characterization and Modelling of Steel Fiber Reinforced Concrete Elements," Ph.D. Thesis, UniversitatPolitècnica de Catalunya, Departamentd'Enginyeria de la Construcció, 2013, 242 pp.

[20] E. K. Sayhood, S. P. Yaakoub, and H. F. Hussien," Nonlinear Finite Element Analysis for Punching Shear Resistance of Steel Fibers High Strength Reinforced Concrete Slabs," Jour. of Engineering and Technology, Vol. 32, No. 6, pp. 1411- 1432, 2014.

[21] T. Puddicome," Finite Element Analysis of Reinforced Concrete and Steel Fiber Reinforced Concrete Slabs in Punching Shear," M. Eng. Thesis, Memorial University of Newfoundland, 2018, Canada.

[22] J. A. O. Barros, and J. A. Figueiras," Flexural Behavior of SFRC: Testing and Modeling,". Jour. of Materials in Civil Engineering, Vol. 11, No. 4, pp. 331-339, 1999.

[23] E. Hinton, and D. R. J. Owen, Finite Element Software for Plates and Shells. Pineridge Press, Swansea, 1984.

[24] R. B. Abdul-Ahad, and J. M. Abbas," Behavior of Steel Fiber Reinforced Concrete under Biaxial Stresses," Proceeding of the International Conference on Recent Developments in Fiber Reinforced Cements and Concrete, Sept. 1989, pp.126-135, Cardiff School of Engineering (U.K.), Edited by Swamy, R.N. and Barr, B., Elsevier Applied Science.

[25] W. S. Yin, C.M. Eric, M. A. Mansur, T. T. C. Hsu," Biaxial Tests of Plain and Fiber Concrete," ACI Material Jour., Vol. 86, No. 3, pp. 236-243, May 1989.

[26] A. T. Leonard, and S. A. Mansur," Biaxial Strength and Deformational Behavior of Plain and Steel Fiber Concrete," ACI Material Jour.., Vol. 88, No. 4, pp. 354-362, July 1991.

[27] A. A. Abdul-Razzak," Nonlinear Finite Element Analysis of Fibrous Reinforced Concrete Structural Members," Ph.D. Thesis, University of Mosul, Iraq, 1996.

[28] A. Bentur, and S. Mindess, "Fibre Reinforced Cementitious Composites,", Tylor and Francis Group, 2nd Ed., New York, 2007.

[29] P. Soroushian, and C. D. Lee," Constitutive Modelling of Steel Fiber Reinforced Concrete under Direct Tension and Compression," Proceedings of the International Conference on Recent Developments in Fiber Reinforced Cements and Concrete, Sept. 18th-20th 1989, pp. 363-377, Cardiff School of Engineering (U.K.), Edited by Swamy, R.N. and Barr, B., Elsevier Applied Science.

[30] D. J. Hannant, " Fibre Cements and Fibre Concretes," Wiley-Interscience, (1978), 1st Ed., New York, 1978.

[31] K. Visalvanich, and A. E. Naaman," Fracture Model for Fiber Reinforced Concrete," ACI Jour., Vol. 80, No. 2, pp. 128-138, Feb. 1983.

[32] S. A. Al-Taan, and M. N. Mahmood, Biaxial Stress-Strain Relationship for Concrete. Proceeding of the 2nd International Conference on Computer Applications in Concrete, pp. C1-C14, Singapore, 28th-29th March 1988.

[33] F. Vecchio, and M. P. Collins, The Modified Compressive - Field Theory for Reinforced Concrete Elements Subjected to Shear." ACI J., 83(2), 1986, pp. 219-231.

[34] L. Cedolin, and S. D. Poli," Finite Element Studies of Shear- Critical R/C Beams," Jour. of Engineering Mech. Div., ASCE, Vol. 103, No 3, pp. 395-410, March 1977.

[35] W. F. Chen," Plasticity in Reinforced Concrete," 1st Ed., J. Ross Publishing, 2007, New York.

[36] R. S. H. Al-Mahaidi," Nonlinear Finite Element Analysis of Reinforced Concrete Deep Members," Ph.D. Thesis, 1978, Dept. of Structural Eng., Cornell University, Ithaca, New York.

[37] E. Onate, E. Hinton, and N. Glover," Techniques for Improving the Performance of Ahmed Shell Elements," Report No. C/R/313/78, 1978, Civil Eng. Dept., University of Wales, Swansea (U.K.).